



# CHF determination for high-heat flux phase change cooling system incorporating both micro-channel flow and jet impingement

Myung Ki Sung, Issam Mudawar\*

Boiling and Two-Phase Flow Laboratory (BTPFL), Purdue University International Electronic Cooling Alliance (PUIECA), Mechanical Engineering Building, 585 Purdue Mall West Lafayette, IN 47907-2088, USA

## ARTICLE INFO

### Article history:

Received 26 March 2008

Received in revised form 11 July 2008

Available online 17 November 2008

## ABSTRACT

This paper explores the subcooled nucleate boiling and critical heat flux (CHF) characteristics of a hybrid cooling module that combines the cooling attributes of micro-channel flow and jet impingement. A test module was constructed and tested using HFE-7100 as working fluid. Increasing the coolant's flow rate and/or subcooling shifted both the onset of boiling (ONB) and CHF to higher heat fluxes and higher wall temperatures. The hybrid module yielded heat fluxes as high as  $1127 \text{ W/cm}^2$ , which is the highest value ever achieved for a dielectric coolant at near atmospheric pressure. It is shown the hybrid cooling configuration involves complex interactions between circular jets and micro-channel flow, and unusual spatial variations of void fraction and liquid velocity. These variations are ascertained using the Developing Homogeneous Layer Model (DHLM) in which the micro-channel flow is described as consisting of a homogeneous two-phase layer along the heated wall and a bulk liquid layer. CHF is determined by a superpositioning technique that consists of dividing the heated wall into two portions, one dominated by jet impingement and the other micro-channel flow. This technique is shown to be highly effective at predicting the CHF data for the hybrid cooling configuration.

© 2008 Elsevier Ltd. All rights reserved.

## 1. Introduction

Many of today's cutting-edge technologies involve the dissipation of large amounts of heat from very small surface areas. Examples include laser and microwave directed energy weapons, radars, X-ray medical devices and hybrid-vehicle power electronics [1]. Failure to remove the dissipated heat can trigger abrupt catastrophic failure. Removing highly concentrated heat loads therefore demands innovative cooling strategies that can deliver very high heat transfer coefficients.

Because of their relatively low convective heat transfer coefficients and linear relationship between heat flux and surface-to-fluid temperature difference, single-phase cooling schemes can result in unacceptably high-temperatures when used to dissipate high fluxes. Two-phase cooling schemes are especially favored for high-heat flux situations because of their high heat transfer coefficients and the steep, nonlinear relationship between heat flux and temperature difference; both of these merits are realized in the nucleate boiling region. These two attributes facilitate the removal of highly concentrated heat loads corresponding to relatively small temperature differences, greatly reducing surface temperature as well as minimizing temperature fluctuations in response to changes in the heat flux. Reducing both temperature and temperature fluctuations is an important operational safe-

guard to ensure the reliability and structural integrity of heat-dissipating devices found in most of the afore-mentioned high-flux applications.

However, two-phase systems are not without drawbacks. They are generally more difficult to implement and more expensive than their single-phase counterparts. This is why two-phase cooling systems are favored only in situations where single-phase systems are deemed incapable of meeting the cooling requirements of given device or system. Also, as indicated earlier, the merits of two-phase cooling are realized only within the nucleate boiling regime. Maintaining cooling performance within this regime requires uninterrupted access of liquid to the heat-dissipating surface to compensate for the evaporated liquid. The liquid access is abundant in the lower heat flux, discrete bubble sub-region of nucleate boiling. However, as the heat flux increases, more vapor is produced and with greater intensity. This causes vapor bubbles to coalesce into larger closely spaced bubbles that begin to restrict the liquid access to the surface. Intense vapor effusion ultimately begins to form discrete vapor blankets that severely restrict the liquid access, greatly compromising cooling effectiveness. This condition is a precursor to critical heat flux (CHF), which is the upper limit for the nucleate boiling region. Increasing the heat flux past CHF triggers a substantial deterioration in the heat transfer coefficient, causing a sudden unsteady escalation in the device temperature that is often large enough to induce catastrophic device failure. The ability to predict CHF is therefore of paramount importance to the integrity of the device.

\* Corresponding author. Tel.: +1 765 494 5705; fax: +1 765 494 0539.  
E-mail address: [mudawar@ecn.purdue.edu](mailto:mudawar@ecn.purdue.edu) (I. Mudawar).



Micro-channel flows are especially prone to saturated CHF. Subcooled CHF is generally associated with high flow rates, high inlet subcoolings and small length-to-diameter ratios. Here, the fluid maintains a predominantly liquid state at the outlet with a relatively small mass of vapor confined to the heated wall. Subcooling plays a vital role in all stages of the vaporization process. Subcooled liquid can absorb an appreciable fraction of the heat supplied from the wall in the form of sensible heat rise before it is converted to vapor. Recently, Qu and Mudawar [9] examined CHF for a heat sink containing parallel rectangular micro-channels using water as working fluid. They showed that interactions between micro-channels reduce CHF compared to a single micro-channel.

Far more numerous studies have been published on CHF in jet impingement than in micro-channel heat sinks. Monde [10] classified CHF regimes for circular jets corresponding to different flow rates and pressures. Monde and Mitsutake [11] extended these findings to systems involving multiple circular jets. For multi-jet systems, they recommended replacing the heater's size in the CHF correlation with a characteristic length for the portion of the surface area that is impacted by a single jet. Qiu and Liu [12] developed correlations for saturated and subcooled CHF for the jet's stagnation zone. Johns and Mudawar [13] showed that the nozzle-to-surface distance has a negligible effect on CHF. Mudawar and Wadsworth [14] developed a cooling module for multiple heat sources that are each cooled by a confined rectangular jet of FC-72. They developed a correlation for CHF that is independent of nozzle-to-surface distance. They also showed CHF is a far stronger function of jet velocity than of flow rate, suggesting CHF can be increased for a given flow rate by decreasing the jet width, albeit at the expense of greater pressure drop. Recently, Meyer et al. [15] extended these findings to a heat source cooled by multiple slot jets of FC-72.

As indicated earlier, the present study concerns a hybrid cooling scheme that combines the cooling attributes of micro-channel flow and jet impingement. In recent studies by the present authors, the single-phase and two-phase performance of this scheme was examined both numerically and experimentally in pursuit of superior cooling performance [16,17]. This study explores the two-phase heat transfer performance and CHF for the hybrid scheme. A CHF superpositioning scheme is presented that consists of applying prior CHF correlations to the portions of

the heated surface that are influenced by jet impingement and micro-channel flow. A theoretical model is also used to determine variations of the two-phase flow characteristics along the micro-channel.

## 2. Experimental methods

### 2.1. Flow loop

Fig. 1 shows a schematic diagram of the flow loop that was assembled to supply HFE-7100 liquid at the desired pressure, temperature and flow rate to the hybrid cooling test module. The spent coolant exiting the test module rejects heat to a secondary refrigeration system via a heat exchanger. A feedback control feature in the refrigeration system regulates the coolant's temperature to within  $\pm 0.5$  °C of the set value. The coolant's flow rate and test module's outlet pressure are controlled by three needle valves. The flow rate is measured by a Coriolis flow meter.

After achieving the desired test module inlet conditions, electrical power is supplied to the test module in small increments. Once steady-state conditions are reached following each power increment, the module's inlet pressure,  $P_{in}$ , outlet pressure,  $P_{out}$ , inlet temperature,  $T_{in}$ , outlet temperature,  $T_{out}$ , test module's temperatures, and heater power,  $P_w$ , are all recorded by an HP3852S data acquisition system for later processing. These measurements are repeated following each power increment, generating a boiling curve up to and including the CHF point. CHF is detected by a sudden unsteady rise in the test module's temperature, which prompts the operator to cut-off electrical power input to preclude any permanent damage to the test module.

Measurement uncertainties associated with the pressure transducers, flow meter, wattmeter, and thermocouples are 0.5%, 0.1%, 0.5%, and 0.3 °C, respectively.

### 2.2. Test module

As shown in Fig. 2(a), the test module consists of a copper heating block, a micro-jet plate, an upper housing, a bottom housing, lower support plates, and 16 cartridge heaters. Five 1-mm wide by 3-mm deep slots are cut equidistantly within a 10-mm width

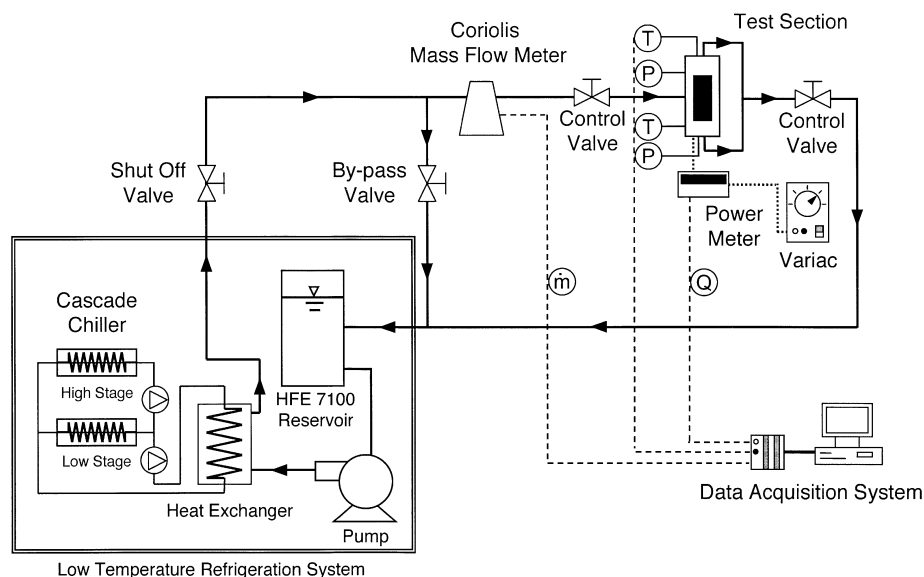


Fig. 1. Schematic of flow loop.

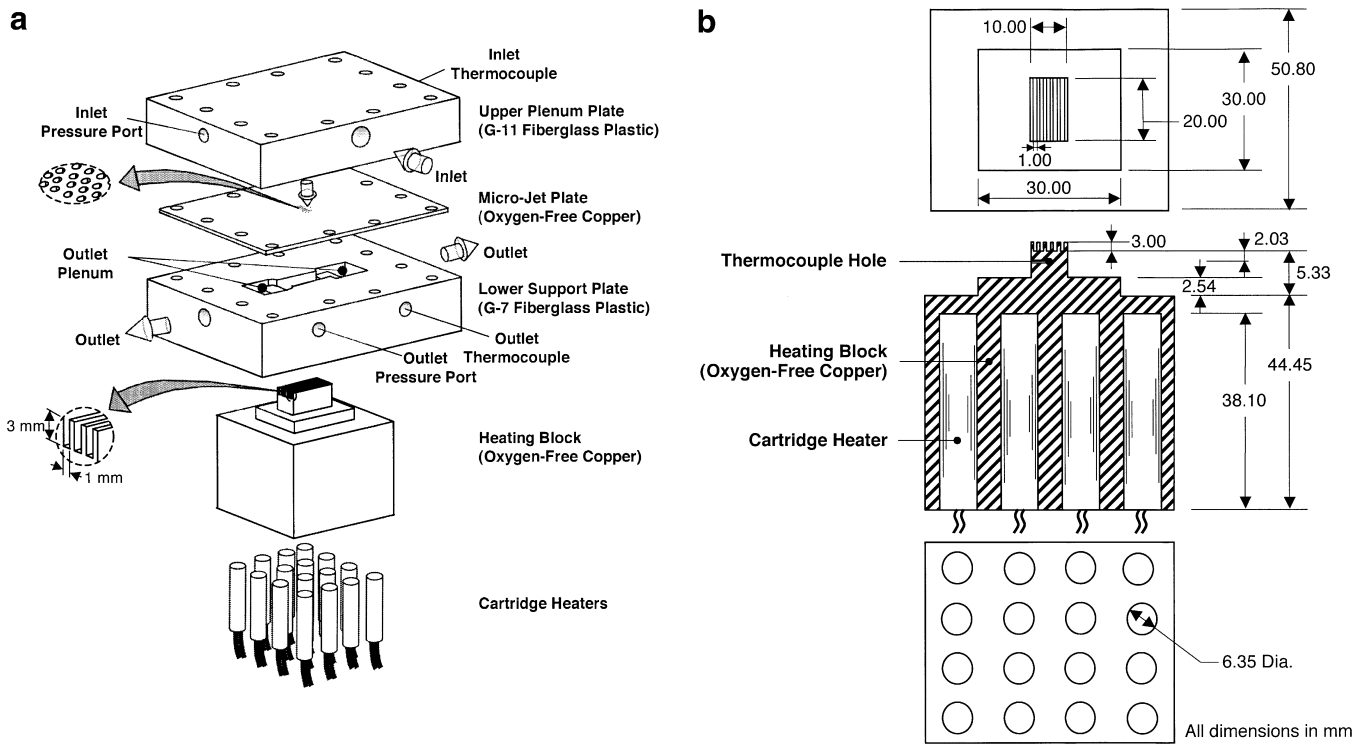


Fig. 2. (a) Test module construction. (b) Details of copper heating block.

of the top  $10 \times 20 \text{ mm}^2$  test surface area of the copper block. Use of the designation “micro-channel” in the present study is based on the premise that the channel influence on departing bubbles is dictated far more by the channel width of 1 mm than by hydraulic diameter.

As shown in Fig. 2(b), the underside of the copper block is bored to accommodate the 16 cartridge heaters, which supply the heat to the test surface. These cartridge heaters are powered by a variable voltage transformer, and their total electrical power input is measured by a Yokogawa WT210 wattmeter. The 1.65-mm thick micro-jet plate is fabricated from oxygen-free copper. Five parallel arrays of circular holes are drilled within the 1-cm width facing the five micro-channels. Fig. 3 shows a unit cell of the cooling geometry, which consists of a single micro-channel, the array of jets that deposit coolant into the same micro-channel, and the surrounding solid. Notice that following impingement, the flow divides in the micro-channel into two equal and opposite parts, each is expelled into one of two plenums in the bottom housing. Table 1 provides key dimensions of the cooling configuration. The upper housing of the test module is fabricated from G-11 fiberglass plastic and the lower housing from high-temperature G-7 fiberglass plastic.

Since the present study is aimed at achieving the highest possible cooling heat fluxes, special care is taken to prevent any thermally induced damage to the test module's parts. A 3-D numerical model was constructed to optimize the shape and dimensions of the copper heating block to enable the dissipation of up to  $1000 \text{ W/cm}^2$  without exceeding the temperature limits of the housing materials or sealant in contact with the copper block. The housing materials are further protected by minimizing contact area with the copper block. Fig. 2(b) shows key dimensions of the optimized copper block. This block is stepped near the top to help ensure uniform temperature across the  $10 \times 20\text{-mm}^2$  test surface area.

Four type-K thermocouples are inserted below the micro-channel's bottom wall to measure the surface temperature. One abso-

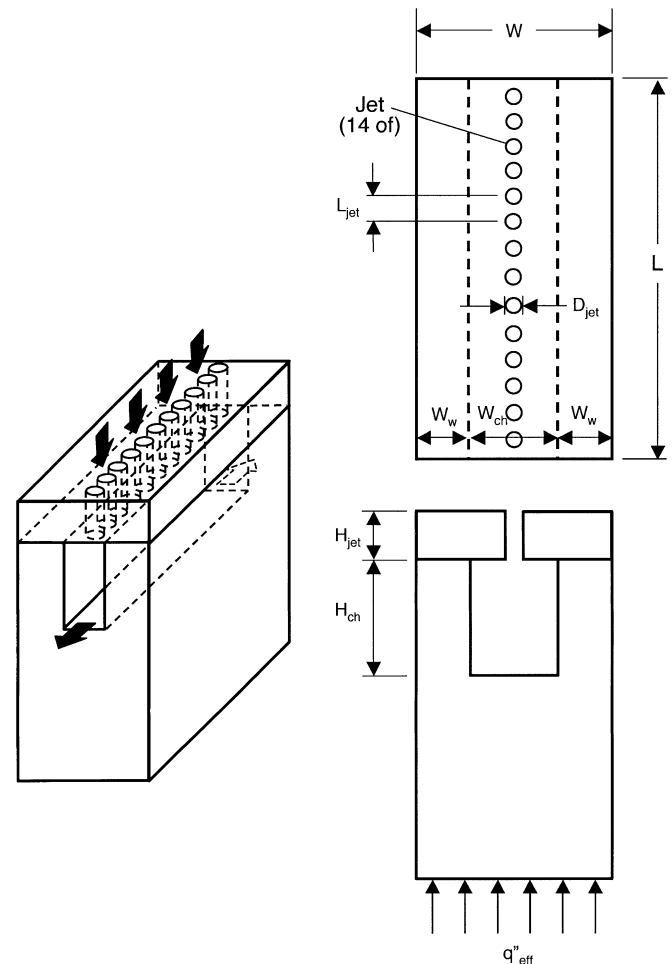


Fig. 3. Schematic of unit cell consisting of micro-circular jets and single micro-channel.

**Table 1**  
Dimensions of unit cell

$H_{ch}$ (mm)	$H_{jet}$ (mm)	$L$ (mm)	$L_{jet}$ (mm)	$W$ (mm)	$W_{ch}$ (mm)	$W_w$ (mm)	$D_{jet}$ (mm)
3.00	1.65	20.00	1.43	1.83	1.00	0.42	0.39

lute pressure transducer and one type-T thermocouple are connected to the inlet plenum in the upper housing. Another absolute pressure transducer and a type-T thermocouple are inserted in the outlet plenums of the bottom housings.

**2.3. Performance parameters**

Jet velocity,  $U_{jet}$ , is determined from the coolant’s volumetric flow rate, which, in turn, is obtained by dividing the mass flow rate measured by the Coriolis flow meter by liquid density.

The heat flux data presented in this paper are based on an effective heat flux,  $q''_{eff}$ , from the test surface area of the copper block, which is calculated by dividing the total electrical power input,  $P_w$ , by the test surface area,  $A_t = 10 \times 20 \text{ mm}^2$ . To estimate heat loss, a 3-D numerical model of the entire test module was constructed and appropriate natural convection boundary conditions applied to its exterior. This model showed heat loss within the nucleate boiling region is less than 4% of the electrical power input. The heat fluxes reported in the present paper are therefore based on the measured electrical power input.

Mean surface temperature,  $\bar{T}_s$ , is determined by area-averaging the micro-channel’s bottom wall temperatures after correcting for the temperature gradient across a distance  $H_{th}$  between the thermocouple and the test surface immediately above

$$\bar{T}_s = \frac{\sum_{tci=1}^4 T_{s,tci} A_{tci}}{A_t} \tag{4}$$

where

$$T_{s,tci} = T_{tci} - \frac{q''_{eff} H_{th}}{k_s} \tag{5}$$

**3. Experimental results**

**3.1. Boiling curve trends**

Boiling curves were generated for broad ranges of inlet temperature and jet velocity as given in Table 2. Fig. 4(a) shows the effects of subcooling on the boiling curve for  $U_{jet} = 1.07 \text{ m/s}$ . The onset of boiling (ONB) is shifted monotonically to higher heat fluxes and higher surface temperatures with increased subcooling. There is also an appreciable enhancement in CHF at higher subcoolings. This increase is the result of the subcooled liquid’s ability to absorb a significant portion of the wall heat in the form of sensible heat rise before undergoing phase change. With subcooled liquid, the size of coalescent vapor bubbles or blankets is greatly reduced by condensation, bringing the bulk liquid closer to the wall.

Fig. 4(b) shows the effects of jet velocity and therefore flow rate on the boiling curve for an inlet temperature of  $T_{in} = -20 \text{ }^\circ\text{C}$ . Like subcooling, increasing the flow rate delays both ONB and CHF to higher heat fluxes and higher surface temperatures. The highest CHF value measured in the present study is  $q''_m = 1080 \text{ W/cm}^2$ . This value was achieved at  $U_{jet} = 5.7 \text{ m/s}$  with a pressure drop of  $\Delta P = 1.2 \text{ bar}$ , which is much smaller than pressure drops encountered in conventional micro-channel flows [7]. It is important to emphasize that this CHF value is by no means an upper heat flux limit for the present hybrid cooling scheme. Fig. 4(a) and (b) shows CHF increases monotonically with increases in subcooling and flow rate, respectively. This points to the ability to achieve even higher CHF values using subcoolings and flow rates that exceed those tested in the present study. As indicated earlier, heat flux is limited by temperature limits of the various materials comprising the test module, and tests had to be aborted to preclude any permanent damage to the test module. Fig. 4(b) shows the test corresponding to  $U_{jet} = 6.50 \text{ m/s}$  yielded an upper flux of  $q''_{eff} = 1127 \text{ W/cm}^2$

**Table 2**  
Experimental operating conditions

Working fluid	Inlet temperature $T_{in}$ ( $^\circ\text{C}$ )	Inlet jet velocity $U_{jet}$ (m/s)	Effective heat flux $q''_{eff}$ ( $\text{W/cm}^2$ )
HFE-7100	-40 to 20	1.05 to 6.50	20.7 to 1.127

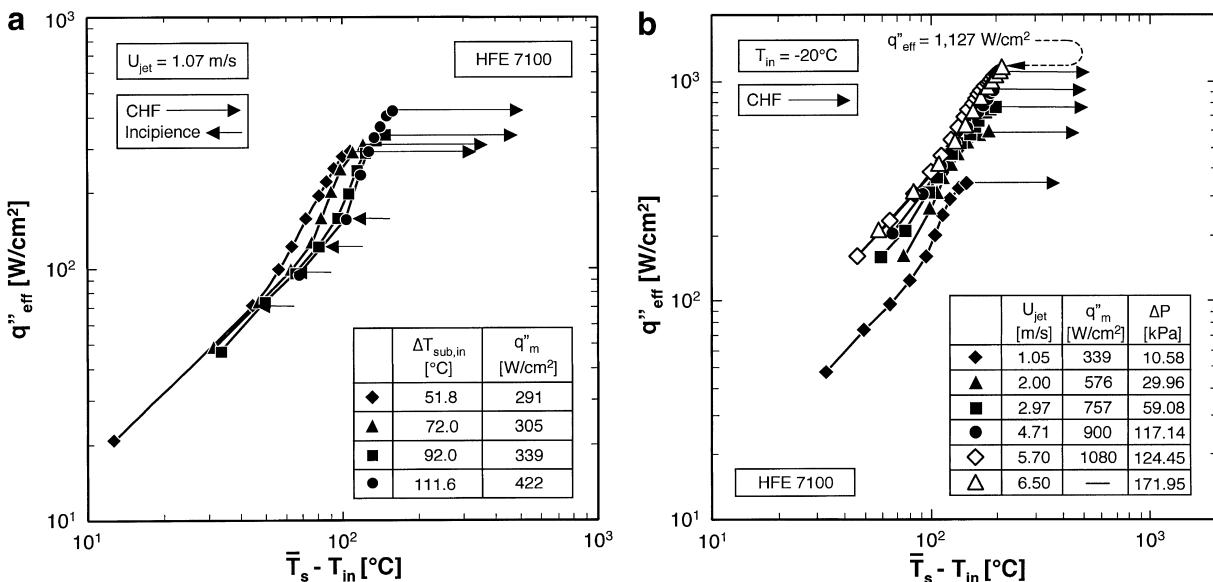


**Fig. 4.** (a) Subcooling effects on boiling curve at  $U_{jet} = 1.04 \text{ m/s}$ . (b) Jet velocity effects on boiling curve at  $T_{in} = -20 \text{ }^\circ\text{C}$ .

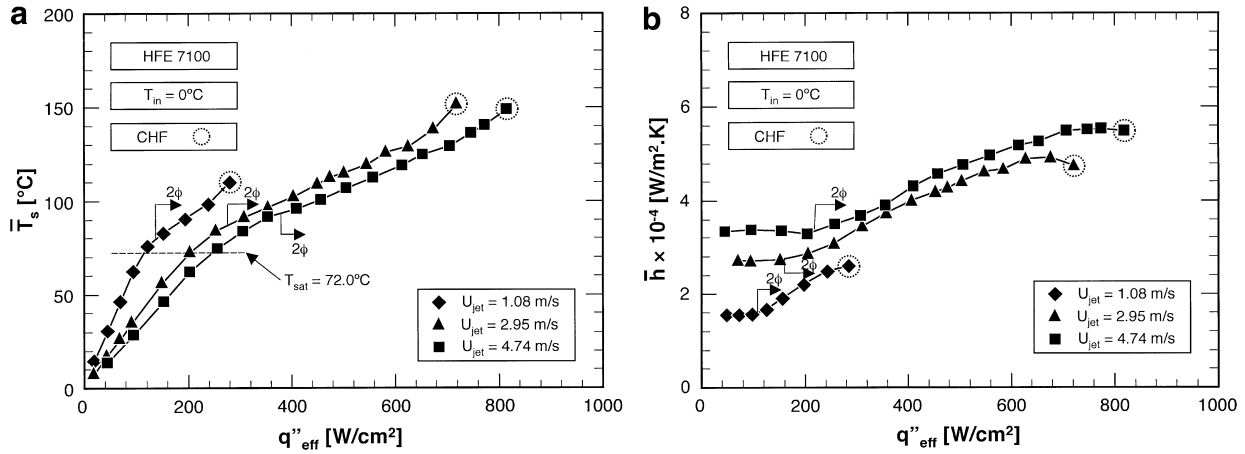


Fig. 5. (a) Variation of channel bottom wall temperature with effective heat flux. (b) Variation of heat transfer coefficient with effective heat flux at  $T_{in} = 0$  °C.

following which the test was intentionally aborted before CHF was achieved. To the authors' knowledge, this heat flux is the highest ever achieved for a dielectric coolant at near atmospheric pressure.

Fig. 5(a) shows the effects of jet velocity on the variation of the area-averaged surface temperature with heat flux for  $T_{in} = 0$  °C. This graph shows that increasing jet velocity delays ONB to a higher heat flux. Fig. 5(b) shows the variation of the heat transfer coefficient with heat flux for the same inlet temperature as Fig. 5(a). The heat transfer coefficient is fairly constant in the single-phase region and increases through most of the nucleate boiling region. Severe vapor coalescence and blanketing at heat fluxes approaching CHF cause a deterioration in the heat transfer coefficient prior to CHF, which is evident for the two higher velocity cases in Fig. 5(b). Not shown is the sudden decrease in the heat transfer coefficient at CHF, which could not be measured because the test module is not designed to endure the full CHF transient, and tests had to be aborted once CHF was detected.

### 3.2. CHF trends

Fig. 6 shows that, while CHF increases monotonically with jet velocity for each of four subcooling cases, the dependence is not very linear, given the fact that CHF is influenced by both jet impingement and channel flow. The next section will discuss means of assessing the contributions of each to the test module's CHF.

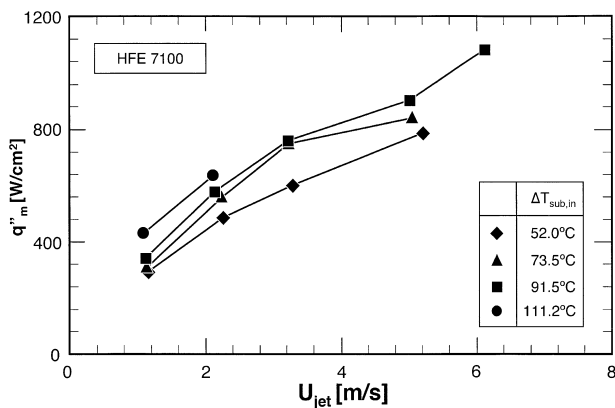


Fig. 6. Variation of CHF with jet velocity for different subcoolings.

## 4. CHF determination

### 4.1. Developing Homogeneous Layer Model (DHLM)

In conventional two-phase micro-channel flow, both quality and void fraction increase monotonically along the micro-channel as liquid is gradually converted to vapor. The present hybrid cooling configuration involves complex interactions between circular jets and micro-channel flow, and unusual spatial variations of quality and void fraction. As illustrated in Fig. 7, the flow pattern is symmetrical relative to the micro-channel's centerline. On either side, jets supply subcooled liquid gradually into the micro-channel, and the flow rate is not constant but increases along the flow direction. It is therefore crucial to ascertain the spatial variations of the key flow parameters in order to determine CHF for the entire module. Achieving this goal is complicated by the fact that the flow along the micro-channel is mostly subcooled, and the liquid and vapor phases do not maintain thermodynamic equilibrium. This precludes the use of conventional parameters such as thermodynamic equilibrium quality to assess the spatial variations of void fraction and flow velocity.

Recently, Lee and Mudawar [18] introduced a new technique to determine spatial variations for subcooled two-phase flow in conventional micro-channels. Using a Developing Homogeneous Layer Model (DHLM), the flow is described as consisting of two layers, a homogeneous two-phase flow layer adjacent to the heated wall and a subcooled liquid core, as illustrated in Fig. 8(a). The model also assumes that, because of the large density differences between liquid and vapor, the velocity of the liquid layer is fairly constant along the micro-channel. Key DHLM equations that are relevant to the present hybrid cooling configuration are discussed here. Further details of the model development can be found in Ref. [18].

As illustrated in Fig. 8(b), mass conservation for a control volume of the micro-channel flow between jets of length  $\Delta z$  requires that

$$\frac{d(\rho_f U_f A_f)}{dz} + K_i = 0 \quad (6a)$$

and

$$\frac{d(G_H A_H)}{dz} - K_i = 0, \quad (6b)$$

where  $U_f$  is the mean velocity of the liquid layer,  $A_f$  the cross-sectional area of the liquid layer,  $G_H (= \rho_H U_H)$  the mass velocity of the homogeneous two-phase layer,  $U_H$  the mean velocity of the

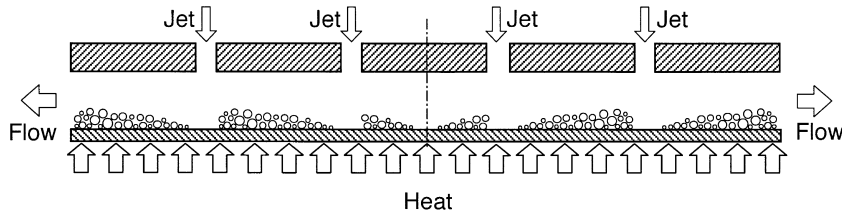


Fig. 7. Schematic representation of vapor growth along micro-channel.

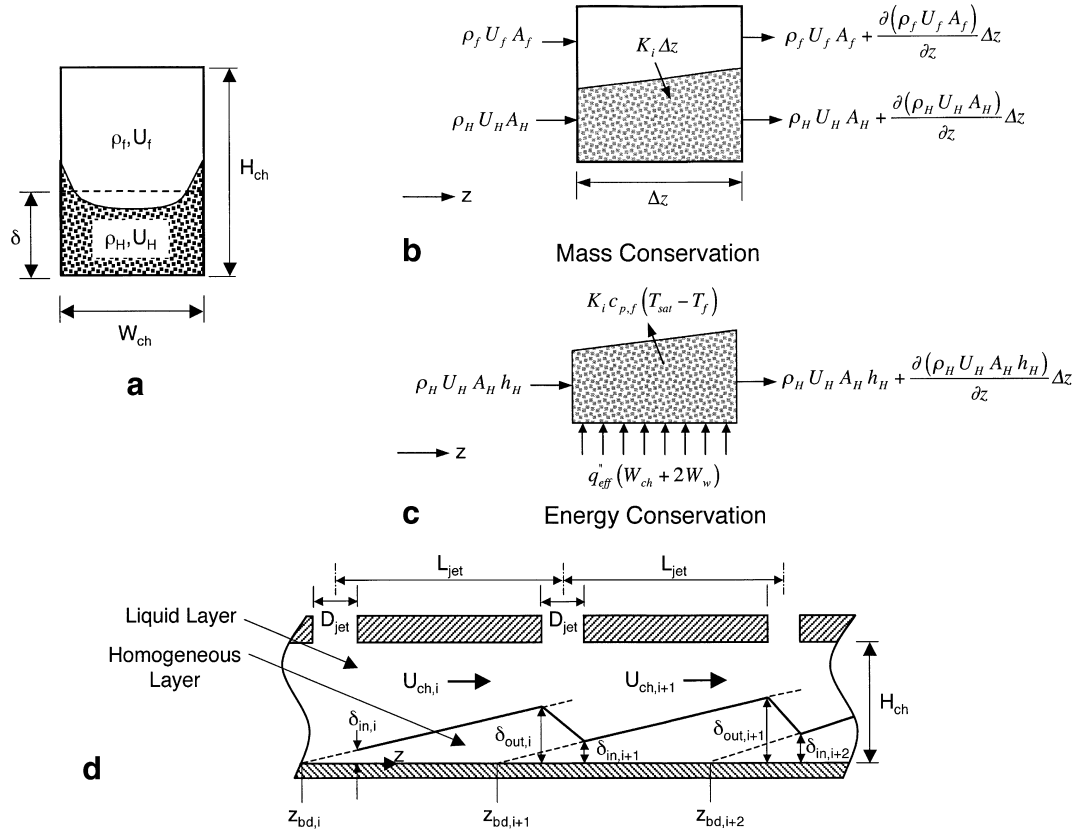


Fig. 8. (a) Cross-sectional representation of Developing Homogeneous Layer Model (DHLM). (b) Mass conservation for liquid and homogeneous layer control volumes. (c) Energy conservation for homogeneous layer control volume. (d) Side view representation of DHLM for hybrid cooling configuration.

homogeneous layer,  $A_H$  the cross-sectional area of the homogeneous layer, and  $K_i$  the rate of mass transfer from the liquid layer to the homogeneous layer per unit distance.

As depicted in Fig. 8(c), energy conservation for the same control volume should account for (i) the portion of the wall heat that increases the temperature of the liquid mass transferred between the liquid layer and the homogeneous layer from  $T_f$  to  $T_{sat}$ , and (ii) a second portion that increases the latent heat of the homogeneous layer.

$$q''_{eff}(W_{ch} + 2W_w) = \frac{d}{dz}(G_H A_H h_H) + K_i c_{p,f}(T_{sat} - T_f), \quad (7)$$

where  $h_H$  is the enthalpy of the homogeneous layer.

As illustrated in Fig. 8(a), the flow areas for the liquid layer and the homogeneous layer can be expressed, respectively, as

$$A_f = W_{ch}(H_{ch} - \delta) \quad (8a)$$

and

$$A_H = W_{ch}\delta, \quad (8b)$$

where  $\delta$  is the thickness of the homogeneous layer. The area derivatives with respect to  $z$  can be expressed as

$$\frac{dA_f}{dz} = -W_{ch} \frac{d\delta}{dz} \quad (9a)$$

and

$$\frac{dA_H}{dz} = W_{ch} \frac{d\delta}{dz}. \quad (9b)$$

Combining Eqs. (6a), (6b), (9a) and (9b), and assuming the velocity of the liquid layer is constant between jets, yield the following relation for the spatial variation of homogeneous layer thickness

$$\frac{d\delta}{dz} = \frac{\delta \frac{dG_H}{dz}}{(\rho_f U_f - G_H)}. \quad (10)$$

As indicated earlier, because vapor is generated along the micro-channel in a subcooled boiling region, thermodynamic equilibrium quality cannot be used to determine the enthalpy of the two-phase layer. According to the DHLM, the enthalpy of the homogeneous layer is expressed as

$$h_H = h_f + x'_H h_{fg}, \quad (11)$$

where  $x'_H$  is an apparent flow quality. Lee and Mudawar [18] reviewed earlier relations to determine  $x'_H$  and found the model by Kroegeer and Zuber [19] well suited for short micro-channels. The apparent flow quality according to the Kroegeer and Zuber model can be expressed as

$$x'_H = \frac{c_{p,f} \Delta T_{\text{sub,in}} (Z^+ - T^*)}{h_{fg} - c_{p,f} \Delta T_{\text{sub,in}} (1 - T^*)}, \quad (12)$$

where

$$Z^+ = \frac{Z - Z_{\text{bd}}}{Z_{\text{sat}} - Z_{\text{bd}}}, \quad (13a)$$

$$T^* = \tanh Z^+, \quad (13b)$$

and  $Z_{\text{bd}}$  and  $Z_{\text{sat}}$  are the axial locations corresponding to bubble departure and thermodynamic equilibrium quality of unity, respectively.

By combining Eqs. (6a), (9a), (9b), (11) and (12) with energy conservation Eq. (7), the spatial variation of the homogeneous layer's mass velocity can be expressed as

$$\frac{dG_H}{dz} = \frac{(\rho_f U_f - G_H) \left\{ q''_{\text{eff}} (W_{\text{ch}} + 2W_w) - W_{\text{ch}} \delta G_H h_{fg} \frac{dx'_H}{dz} \right\}}{\rho_f U_f W_{\text{ch}} \delta [h_H + c_{p,f} (T_{\text{sat}} - T_f)]}. \quad (14)$$

The spatial variation of the homogeneous layer's thickness can be obtained by substituting Eq. (14) into Eq. (10).

$$\frac{d\delta}{dz} = \frac{q''_{\text{eff}} (W_{\text{ch}} + 2W_w) - W_{\text{ch}} \delta G_H h_{fg} \frac{dx'_H}{dz}}{\rho_f U_f W_{\text{ch}} [h_H + c_{p,f} (T_{\text{sat}} - T_f)]}. \quad (15)$$

Eqs. (14) and (15) are coupled ordinary differential equations. The homogeneous layer's thickness must satisfy the following boundary conditions:

$$\delta = \begin{cases} 0 & \text{at } z = -Z_{\text{bd}} \\ H_{\text{ch}} & \text{at } z = Z_{\text{sat}} \end{cases}. \quad (16)$$

The location of saturated boiling,  $Z_{\text{sat}}$ , can be determined with the aid of a simple energy balance.

$$Z_{\text{sat}} = \frac{\rho_f U_f W_{\text{ch}} H_{\text{ch}} c_{p,f} (T_{\text{sat}} - T_f)}{q''_{\text{eff}} (W_{\text{ch}} + 2W_w)}. \quad (17)$$

The location of bubble departure,  $Z_{\text{bd}}$ , is calculated from

$$Z_{\text{bd}} = - \left[ Z_{\text{sat}} - \Delta T_{\text{sub,bd}} \frac{\rho_f U_f W_{\text{ch}} H_{\text{ch}} c_{p,f}}{q''_{\text{eff}} (W_{\text{ch}} + 2W_w)} \right], \quad (18)$$

where, from [20]

$$\Delta T_{\text{sub,bd}} = \frac{q''_{\text{eff}}}{h_{\text{bd}}}. \quad (19)$$

The heat transfer coefficient at the point of bubble departure,  $h_{\text{bd}}$ , in the micro-channel can be determined using an iterative procedure that seeks to satisfy the boundary conditions of the homogeneous layer's thickness given by Eq. (16).

The above DHLM development concerns the micro-channel segments between jets. As illustrated in Fig. 8(d), the thickness,  $\delta$ , of the homogeneous layer increases along the micro-channel until it encounters the next jet. This second jet deposits additional fluid, which increases the coolant's mass flow rate for the next micro-channel segment. A new liquid layer velocity must be used for the second segment to account for the jet fluid. This new velocity can be determined from mass conservation

$$U_{\text{ch},i+1} = \frac{\rho_f U_{\text{ch},i} W_{\text{ch}} (H_{\text{ch}} - \delta_{\text{out},i}) + \rho_f U_{\text{jet}} A_{\text{jet}}}{\rho_f W_{\text{ch}} (H_{\text{ch}} - \delta_{\text{in},i+1})}. \quad (20)$$

The heat transfer coefficient at bubble departure,  $h_{\text{bd}}$ , is recalculated for the micro-channel segment downstream from the jet using the updated liquid layer velocity to once again satisfy the boundary conditions given by Eq. (16).

Fig. 9(a) and (b) show predicted variations of liquid layer velocity and homogeneous layer thickness along the micro-channel for  $T_{\text{in}} = -20^\circ\text{C}$  and  $U_{\text{jet}} = 3.2$  and  $6.1$  m/s, respectively. In both cases, the liquid layer velocity increases along the micro-channel. While the thickness of the homogeneous layer increases between jets, its overall magnitude decreases along the micro-channel. Comparing Fig. 9(a) and (b) shows increasing the jet velocity and therefore the coolant's flow rate increase the liquid layer velocity and, to a lesser extent, decrease the thickness of the homogeneous layer.

As discussed in the next section, the liquid layer velocity given by Eq. (20) is key to assessing the contribution of the micro-channel flow to CHF.

#### 4.2. CHF prediction procedure

The strategy used in predicting CHF for the hybrid cooling configuration is to superimpose the contributions of jet impingement and micro-channel flow. In other words, the heated area is divided into two portions, one dominated by jet impingement and the other by micro-channel flow. As illustrated in Fig. 10(a), the first portion consists of the stagnation zones of the jets and surrounding vicinity, while the second is comprised of the remaining micro-channel flow areas between jets.

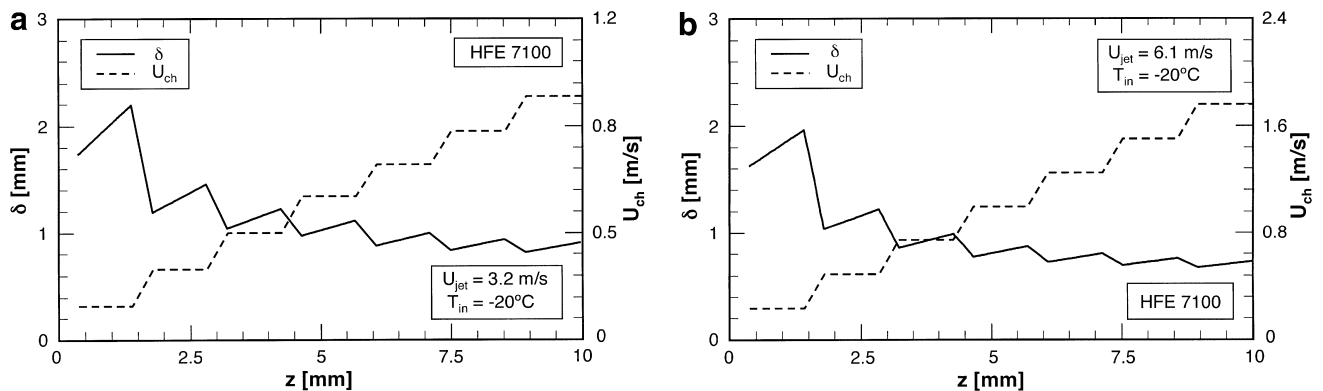


Fig. 9. Variations of homogeneous layer thickness and liquid layer velocity along micro-channel for  $T_{\text{in}} = -20^\circ\text{C}$  at (a)  $U_{\text{jet}} = 3.2$  m/s and (b)  $U_{\text{jet}} = 6.1$  m/s.

To determine CHF for the hybrid cooling configuration, separate CHF correlations are used for the jet impingement and micro-channel portions of the heat wall. For jet impingement, the correlation by Monde and Mitsutake [11] is used

$$\frac{q''_{mw}}{q''_{mw,sat}} = \frac{1 + \sqrt{1 + 4CJa}}{2}, \quad (21)$$

where

$$\frac{q''_{mw,sat}}{\rho_f U_{jet} h_{fg}} = 0.221 \left(\frac{\rho_f}{\rho_g}\right)^{0.645} \left(\frac{2\sigma}{\rho_f U_{jet}^2 (l - D_{jet})}\right)^{0.343} \left(1 + \frac{l}{D_{jet}}\right)^{-0.364} \quad (22)$$

$$C = \frac{0.95 \left(\frac{D_{jet}}{l}\right)^2 \left(1 + \frac{l}{D_{jet}}\right)^{0.364}}{\left(\frac{\rho_f}{\rho_g}\right)^{0.43} \left(\frac{2\sigma}{\rho_f U_{jet}^2 (l - D_{jet})}\right)^{0.343}}, \quad (23)$$

$$Ja = \left(\frac{\rho_f}{\rho_g}\right) \left(\frac{c_{p,f} \Delta T_{sub,in}}{h_{fg}}\right), \quad (24)$$

$l$  is the characteristic length of the heated surface (the length of a square heater for single jet case), and  $q''_{mw}$  is CHF based on the wetted area. This correlation is highly effective for circular impinging jets since it is equally accurate in predicting data for a single jet

or multiple jets; it is also valid for coolants with drastically different thermophysical properties. For systems involving multiple jets, Monde and Mitsutake recommended that instead of representing the length of the heated surface, the characteristic length,  $l$ , in their CHF correlation be replaced by twice the longest length between the center of a jet's stagnation zone and the edge of the portion of the heated area that is impacted by the same jet. For the present hybrid cooling configuration,  $l$  is set equal to twice the distance from the center of the jet's stagnation zone to the furthest point along the micro-channel's sidewall.

$$\frac{l}{2} = \sqrt{\left(\frac{W_{ch}}{2}\right)^2 + H_{ch}^2}. \quad (25)$$

For the micro-channel portion of the heated wall, the correlation by Mudawar and Bowers [21] is used because of its suitability to subcooled micro-channel flow. For very short lengths, their correlation can be expressed as

$$\frac{q''_{mw}}{\rho_f U h_{fg}} = 0.104 \left(\frac{\rho_f}{\rho_g}\right)^{-0.29} \left(\frac{\rho_f U^2 L}{\sigma}\right)^{-0.24} \left[1 + 0.4 \frac{c_{p,f} \Delta T_{sub,o}}{h_{fg}}\right], \quad (26)$$

where  $q''_{mw}$  is CHF based on the channel's wetted area. For the hybrid cooling configuration, the inlet velocity,  $U$ , and tube length,  $L$ , in Eq. (26) are replaced for each micro-channel segment between jets by  $U_{ch,i}$  and  $L_{jet} - D_{jet}$ , respectively. The outlet subcooling,  $\Delta T_{sub,o}$ , in Eq. (26) is calculated with assuming a linearly increasing liquid temperature from the center of the micro-channel to the outlet based on measured inlet and outlet temperatures.

Once CHF values are determined for all the jet impingement and micro-channel segments of the flow area, CHF for the entire test module is calculated by area-averaging these values over the top test surface area,  $A_t$ , of the module.

$$\begin{aligned} & [(W_{ch} + 2W_w)L_{jet}]q''_m \\ &= [2(W_{ch} + H_{ch})(L_{jet} - D_{jet})] \\ & \times \frac{1}{N} \sum_{i=1}^N q''_{mw,i} \Big|_{\text{Mudawar}} \\ & \quad \& \text{Bowers} \\ & + \left[2(W_{ch} + H_{ch})D_{jet} - \frac{\pi D_{jet}^2}{4}\right] q''_{mw} \Big|_{\text{Monde}} \\ & \quad \& \text{Mitsutake} \end{aligned} \quad (27)$$

Fig. 10(b) shows this superpositioning technique is very effective at predicting the HFE-7100 CHF data, evidenced by a mean absolute error of 15.2%.

**5. Conclusions**

This study examined the two-phase heat transfer performance of a hybrid cooling scheme that combines the cooling attributes of micro-channel flow and jet impingement. A test module was constructed and tested using highly subcooled HFE-7100 to explore nucleate boiling and CHF trends. A two-phase flow model was used to ascertain liquid velocity variations along the micro-channel. Using the calculated velocities, a superpositioning technique was developed to determine CHF for the hybrid cooling configuration. Key findings from the study are as follows:

- (1) Increasing flow rate and/or subcooling shifts both the onset of boiling (ONB) and CHF to higher heat fluxes and higher temperatures. However, data appear to converge in the nucleate boiling region. The highest CHF value of 1080 W/cm<sup>2</sup> was measured with a jet velocity of 5.70 m/s and inlet temperature of -20 °C. The upper heat flux value

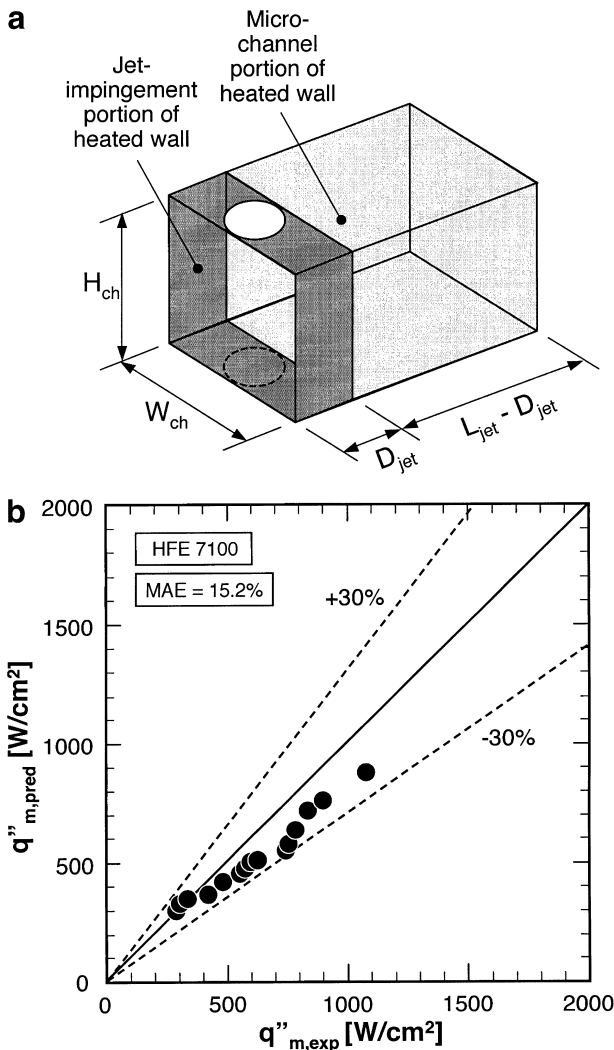


Fig. 10. (a) Partitioning of one segment of the heated wall into jet impingement and micro-channel flow portions. (b) Comparison of CHF data and predictions based on CHF superpositioning scheme.

measured in this study is  $1127 \text{ W/cm}^2$ , which corresponds to a jet velocity of  $6.50 \text{ m/s}$  and  $-20 \text{ }^\circ\text{C}$  inlet temperature; this test was intentionally aborted prior to CHF to protect the test module against burnout. To the authors' knowledge, these heat flux values are the highest ever achieved for a dielectric coolant at near atmospheric pressure.

- (2) The hybrid cooling configuration involves complex interactions between circular jets and micro-channel flow, and unusual spatial variations of quality and void fraction. With the subcooled liquid supplied gradually by the jets, the flow rate is not constant but increases along the micro-channel. Following the assumptions of the Developing Homogeneous Layer Model (DHLM), the micro-channel flow is described as consisting of a homogeneous two-phase layer along the heated wall and a bulk liquid layer. This model is highly effective at determining the complex liquid velocity variations along the micro-channel.
- (3) CHF is determined with a superpositioning technique that consists of dividing the heated wall into two portions, one dominated by jet impingement and the other micro-channel flow. This technique utilizes the DHLM to determine liquid velocity for each segment of the micro-channel between jets. A prior CHF correlation by Monde and Mitsutake is applied to the jet impingement portion, and a CHF correlation by Bowers and Mudawar to the micro-channel portion. This superpositioning technique is shown to be highly effective at predicting the CHF data for the hybrid cooling configuration.

### Acknowledgement

The authors are grateful for the financial support of the Office of Naval Research (ONR).

### References

- [1] I. Mudawar, Assessment of high-heat-flux thermal management schemes, *IEEE Trans. Component Packaging Tech.* 24 (2001) 122–141.
- [2] Y. Katto, Critical heat flux in forced convective flow, *Proc. ASME/JSM Thermal Eng. Joint Conf. Hawaii* 3 (1983) 1–10.
- [3] Y. Haramura, Y. Katto, A new hydrodynamic model of critical heat flux applicable to both pool and forced convection boiling on submerged bodies in saturated liquids, *Int. J. Heat Mass Transfer* 26 (1983) 389–399.
- [4] I. Mudawar, T.A. Incropera, F.P. Incropera, Boiling heat transfer and critical heat flux in liquid films falling on vertically-mounted heat sources, *Int. J. Heat Mass Transfer* 30 (1987) 2083–2095.
- [5] I. Mudawar, D.E. Maddox, Critical heat flux in subcooled flow boiling of fluorocarbon liquid on a simulated electronic chip in a vertical rectangular channel, *Int. J. Heat Mass Transfer* 32 (1989) 379–394.
- [6] M.B. Bowers, I. Mudawar, High flux boiling in low flow rate, low pressure drop mini-channel and micro-channel heat sinks, *Int. J. Heat Mass Transfer* 37 (1994) 321–332.
- [7] I. Mudawar, M.B. Bowers, Ultra-high heat flux (CHF) for subcooled water flow boiling-I: CHF data and parametric effects for small diameter tubes, *Int. J. Heat Mass Transfer* 42 (1999) 1405–1428.
- [8] D.D. Hall, I. Mudawar, Ultra-high critical heat flux (CHF) for subcooled water flow boiling-II: high-CHF database and design equations, *Int. J. Heat Mass Transfer* 42 (1999) 1429–1456.
- [9] W. Qu, I. Mudawar, Measurement and correlation of critical heat flux in two-phase micro-channel heat sinks, *Int. J. Heat Mass Transfer* 45 (2002) 2549–2565.
- [10] M. Monde, Critical heat flux in saturated forced convection boiling on a heated disk with an impinging jet, *ASME J. Heat Transfer* 109 (1987) 991–996.
- [11] M. Monde, Y. Mitsutake, Critical heat flux in forced convective subcooled boiling with multiple impinging jets, *ASME J. Heat Transfer* 118 (1996) 241–243.
- [12] Y. Qiu, Z. Liu, Critical heat flux in saturated and subcooled boiling for R-113 jet impingement on the stagnation zone, *J. Appl. Thermal Eng.* 25 (2005) 2367–2378.
- [13] M.E. Johns, I. Mudawar, An ultra-high power two-phase jet-impingement avionic clamshell module, *ASME J. Electron. Packaging* 118 (1996) 264–270.
- [14] I. Mudawar, D.C. Wadsworth, Critical heat flux from a simulated chip to a confined rectangular impinging jet of dielectric liquid, *Int. J. Heat Mass Transfer* 34 (1991) 1465–1479.
- [15] M.T. Meyer, I. Mudawar, C.E. Boyack, C.A. Hale, Single-phase and two-phase cooling with an array of rectangular jets, *Int. J. Heat Mass Transfer* 49 (2006) 17–29.
- [16] M.K. Sung, I. Mudawar, Single-phase hybrid micro-channel/micro-jet impingement cooling, *Int. J. Heat Mass Transfer* 51 (2008) 4342–4352.
- [17] M.K. Sung, I. Mudawar, Single-phase and two-phase heat transfer characteristics of low temperature hybrid micro-channel/micro-jet impingement cooling module, *Int. J. Heat Mass Transfer* 51 (2008) 3882–3895.
- [18] J. Lee, I. Mudawar, Experimental investigation and theoretical model for subcooled flow boiling pressure drop in micro-channel heat sinks, *ASME J. Electron. Packaging*, submitted for publication.
- [19] P.G. Kroeger, N. Zuber, An analysis of the effects of various parameters on the average void fractions in subcooled boiling, *Int. J. Heat Mass Transfer* 11 (1968) 211–213.
- [20] P. Saha, N. Zuber, Point of net vapor generation and vapor void fraction in subcooled boiling, in: *Heat Transfer*, vol. 4, *Proc. Int. Heat Transfer Conf.*, Tokyo, 1974, pp. 175–179.
- [21] M.B. Bowers, I. Mudawar, Parametric study of ultra-high CHF in highly subcooled water flow inside small diameter tubes, in: J.C. Chen, Y. Fujita, F. Mayinger, R.A. Nelson (Eds.), *Convective Flow Boiling*, Taylor & Francis, Washington, DC, 1996, pp. 117–122.